(034)

Design and Modal Analysis of a Large Deployable Solar Sail System based on Flasher Origami Structure and CFRP Boom

Zijie Chen [1,2], Wenyao Zhang [2], Hongyi Xie [1], Fuqiang Duan [3], Hongwei Guo [2], Penghao Chen [1,4] and Franco Bernelli-Zazzera [1]

[1] Politecnico di Milano, Milan, Italy
[2] Harbin Institute of Technology, Harbin, China
[3] National University of Defence Technology, Changsha, China
[4] Jiangnan University, Wuxi, China
E-mail: Hongyi.Xie@polimi.it

Summary: This paper introduces a new type of solar sail spacecraft structure. The structure can realize the reliable deployment of ultra-large solar sails and can provide sufficient tension to form a stable tensile structure. The spacecraft includes a solar sail with reflectivity control devices (RCDs) for precise orbit and attitude control, a powerful supercomputer for large-scale offline analysis, and a powerful rotating laser communication system for reliable signal transmission to a relay satellite in geostationary orbit (GSO). The solar sail structure includes an origami-based membrane structure and deployable CFRP (Carbon Fiber Reinforced Polymer) boom. The foldable membrane structure is a Flasher origami-based structure that can be easily deployed and retracted over a large area. The deploying mode and the degree of freedom of the origami pattern was analyzed. Moreover, the finite element method was used to analyze the modes of the solar sail structure and calculate the frequency and vibration mode to ensure the reliability of the structural design.

Keywords: Solar sail, Membrane structure, Deployable CFRP boom, Flasher origami, Modal analysis.

1. Introduction

Industry 4.0 and 5.0 are accelerating intelligent automation and decentralization, driving an unprecedented surge in computational demands and energy consumption [1]. The reliance on fossil fuels and low-efficiency terrestrial solar power exacerbates these challenges. Meanwhile, declining launch costs, led by reusable rockets [2], make space-based supercomputing viable for non-time-sensitive, large-scale tasks like AI model training, blockchain processing, and scientific simulations. Instead of straining Earth's power grids, a sustainable alternative is deploying supercomputing platforms in space, powered by large solar sails with integrated thin-film solar cells, ensuring continuous solar energy utilization [3].

Existing initiatives like Lumen Orbit's AI in Space and Thales Alenia's ASCEND project explored space-based AI model-training and data centers [4], but their low Earth orbit (LEO) designs require large-scale in-space assembly [5] and frequent station-keeping [6], suffer power losses in Earth's shadow, and face interference from satellite constellations [7-8] and space debris [9]. In contrast, the proposed Lagrange Point Solar Sail Supercomputer (SSC) at the Sun-Earth L1 point enjoys uninterrupted solar power and requires no propellant for station-keeping [3]. The SSC integrates an origami-based deployable solar sail, CFRP booms, a high-performance supercomputer (e. g. Frontier supercomputer [10]), and a laser communication system for uninterrupted operations. Unlike traditional spacecraft, the SSC relies on numerous Reflectivity Control Devices (RCDs) for precise attitude and thrust control, increasing failure risks. Building on previous fault-tolerant control research [11-12], we proposed two fault-tolerant mechanisms for solar sail RCD failures in [13-14], enhancing SSC mission safety and ensuring long-term stability in deep space. Shielded in the sail's shadow, the supercomputer minimizes thermal regulation needs, while a rotating laser system ensures seamless data transmission via relay satellites in Geostationary Orbit (GSO). This scalable, autonomous system offers a zero-carbon alternative to Earth-based data centers, revolutionizing AI, scientific research, and industrial computing while eliminating fossil fuel dependence and carbon emissions.

To achieve reliable deployment and structural stability, the SSC leverages an origami-based solar sail design, which provides lightweight, high-stiffness, and efficient folding/expansion characteristics. In recent years, origami structures such as Miura-ori, Flasher, Waterbomb, and Kresling have been widely applied in large-scale deployable space structures [15]. Among them, the Flasher origami structure, a single-degree-of-freedom rotational deployment mechanism, is particularly well-suited for solar sail applications [16]. Similar to JAXA's IKAROS, which utilized rotational deployment for sail expansion [17], the Flasher-based solar sail structure in this study enables rapid and controlled deployment while significantly reducing mechanical complexity. Additionally, this design incorporates a deployable CFRP tension structure, which enhances system stiffness and ensures stable deployment. Furthermore, this paper analyzes the structural modes of the solar sail under different

prestress conditions, providing insights into its dynamic behavior and deployment reliability.

2. Configuration Design

Flasher origami is a type of rotationally wound folding configuration that features an exceptionally high folding ratio, as its collapsed size corresponds to the size of its central polygon. This origami structure unfolds either in a clockwise or counterclockwise direction, depending on the orientation of its diagonal creases. As early as 1974, Scheel designed a similar structure for use in solar sails [18]. To date, flasher origami has evolved into numerous configurations, as shown in Fig. 1.

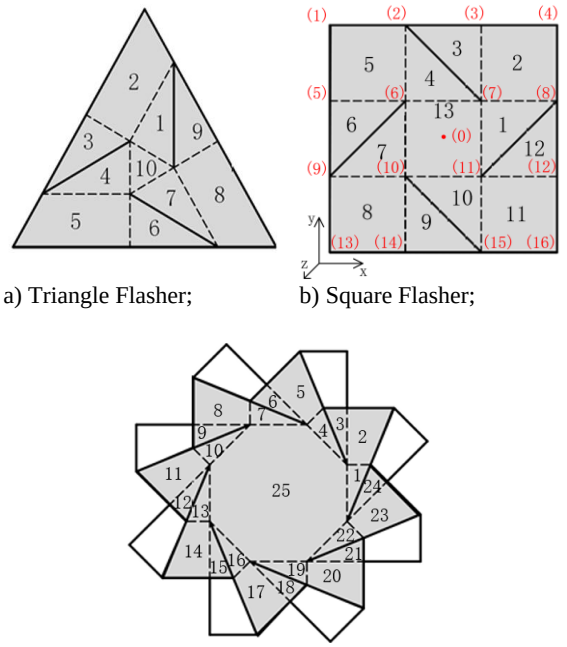

a) Triangle Flasher; b) Square Flasher;

c) Octagon Flasher

Fig. 1. Flasher origami patterns.

Flasher origami patterns vary depending on the shape of the central design. As the central polygon changes, the pattern gradually becomes more complex, and the overall area roughness increases (Fig. 1. c)), which may adversely affect the attitude control of the solar sail. Hence, considering various factors, Flasher patterns with a square central design are more suitable as folding configurations for solar sails.

A single-layer square Flasher origami pattern, as shown in Fig. 1. b), consists of 13 folding planes and 16 nodes. Based on the degree of freedom analysis method for Miura origami proposed in [19], a similar analysis can be applied to Fig. 1. b). By treating it as an equivalent spatial linkage system and imposing additional geometric constraints on the equivalent linkage members, the degrees of freedom can be further evaluated.

$$\begin{aligned}
&l_{(1),(2)},\cdots,l_{(5),(1)} = constant \\
&l_{(2),(7)},\cdots,l_{(9),(6)} = constant && \text{(Length)} \\
&\left[\boldsymbol{v}_{(1),(5)},\boldsymbol{v}_{(1),(6)},\boldsymbol{v}_{(1),(2)}\right] = 0 \\
&\vdots && \text{(Surface)} \\
&\left[\boldsymbol{v}_{(7),(6)},\boldsymbol{v}_{(7),(2)},\boldsymbol{v}_{(6),(2)}\right] = 0 && (1) \\
&x_1, y_1, z_1, x_2, z_2, z_4 = 0 && \text{(Boundary)} \\
&\angle\left(l_{(0),(2)},l_{(0),(8)}\right) = constant \\
&\vdots && \text{(Rotation)} \\
&\angle\left(l_{(0),(9)},l_{(0),(2)}\right) = constant
\end{aligned}$$

where, $l_{(i),(j)}$ represents the length of the line between nodes (*i*) and (*j*), $\boldsymbol{v}_{(i),(j)}$ represents the vector pointing from node (*i*) to node (*j*), $\angle\left(l_{(i),(j)},l_{(i),(k)}\right)$ represents the angle formed by points (*i*), (*j*), (*k*).

The above constraints can be uniformly expressed as constraint equations:

$$F\left(x_1, y_1, z_1, \cdots, x_n, y_n, z_n\right) = 0 \quad k = 1, 2, \cdots, m \quad (2)$$

where, *n* is the number of system nodes and *m* is the number of constraint equations. Based on the Jacobian matrix, the kinematics of the origami structure is solved and the first-order derivative of Eq. (2) is obtained:

$$\boldsymbol{A}\dot{\boldsymbol{X}} = 0 \quad (3)$$

where, *A* is the Jacobian matrix, which is also the first-order influence matrix, and *X* is the node matrix of the pattern. Solving Eq. (3) yields the results shown in Table 1.

Table 1. First-order analysis of single-layer pattern.

Constraints	Size of *A*	Nullity
Length	(28,48)	19
Surface	(33,48)	14
Boundary	(40,48)	6
Rotation	(46,48)	2

For rotationally wound folding configurations, the dimension of the null space of the rotational constraint equations corresponds to the degrees of freedom for rigid rotational deployment. In other words, the single-layer square Flasher origami structure has two degrees of freedom for rigid rotational deployment, which are associated with the rotational motions when its four diagonal creases alternately act as mountain and valley folds.

Due to the limited number of folds, this single-layer square Flasher origami pattern is challenging to apply to large-scale solar sails. Further topological modifications are required, such as expanding it into a

two-layer pattern. Using a similar degree of freedom analysis method, this expanded structure can be further analyzed.

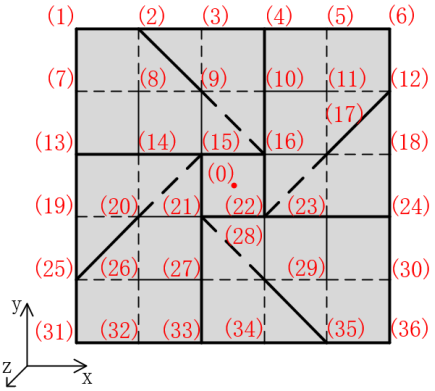

Fig. 2. Double layer square flasher pattern.

This pattern still requires consideration of length constraints, diagonal constraints, surface constraints, boundary constraints, and rotational symmetry constraints. By substituting the new node information into Eq. (1) - (3), the first-order analysis results can be obtained, as shown in Table 2.

Table 2. First-order analysis of double-layer pattern.

Constraints	Size of A	Nullity
Length	(76,108)	39
Surface	(85,108)	23
Boundary	(92,108)	16
Rotation	(104,108)	4

The null space dimension of the rotational symmetry constraint equations for the double-layer pattern is 4, indicating that it has 4 degrees of freedom and supports 4 distinct folding modes, as shown in Fig. 3.

Combined with the analysis results of the single-layer pattern and double-layer pattern, it is evident that for square Flasher patterns, their degrees of freedom satisfy the following equation:

$$M = 2^n \tag{4}$$

where, n represents the number of layers in Flasher patterns. Furthermore, to enhance the folding ratio of the pattern when applied to solar sails, its diagonal creases must satisfy the requirement that mountain folds and valley folds alternate. In this case, the number of layers in the solar sail pattern can be determined by the following equation:

$$n = \frac{l/l_0 - 1}{2} \tag{5}$$

where, l represents the edge length of the fully deployed solar sail and l_0 represents the edge length of the fully folded solar sail.

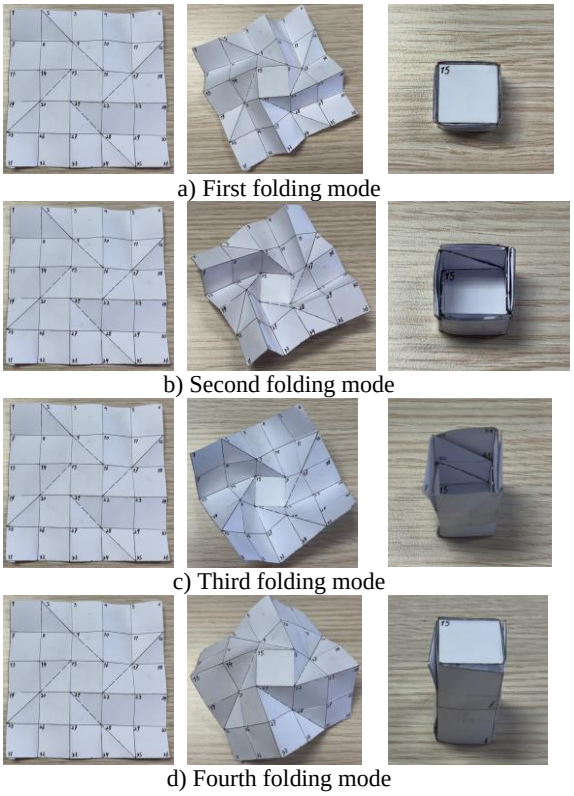

a) First folding mode

b) Second folding mode

c) Third folding mode

d) Fourth folding mode

Fig. 3. Four modes of double layer square flasher pattern.

To ensure the successful deployment of the solar sail, it is necessary to design an appropriate deployment mechanism. Elastic rod mechanisms based on carbon fiber composite materials offer high deployment stiffness while being lightweight and having a minimal stowed envelope. These mechanisms are now widely used in large deployable solar sail structures. Additionally, elastic rods can provide sufficient tension to the solar sail membrane, eliminating creases and wrinkles that may form after the folding pattern unfolds. A structural diagram comprising the solar sail, deployable CFRP boom, supercomputer, and array is shown in Fig. 4.

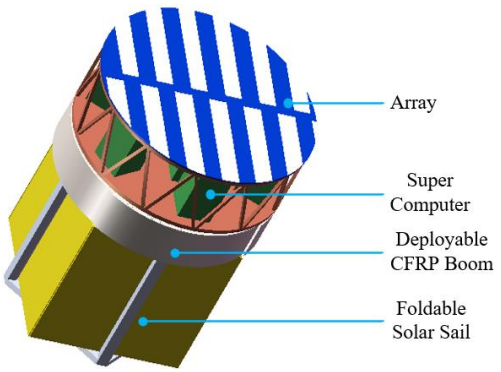

Fig. 4. Deployable solar sail contains supercomputer.

Additionally, the deployment process of the entire solar sail system is illustrated in Fig. 5, where the solar sail's origami structure is exemplified by a double-layer square Flasher pattern.

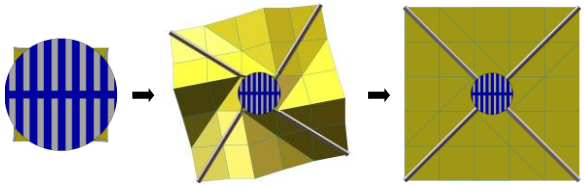

Fig. 5. Deploying process of solar sail system.

3. Modal Analysis

After completing the design of the solar sail structure, it is necessary to analyze its modes after deployment. If the structural stiffness is insufficient, there is a risk of structural failure. In this study, the finite element method is used to analyze the solar sail structure, and the results of its first-order vibration mode are shown in Fig. 6.

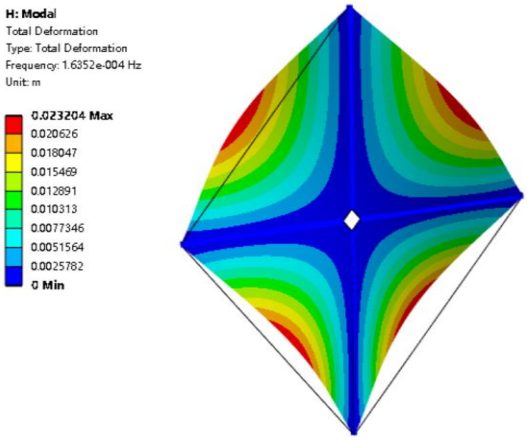

Fig. 6. First-order vibration mode of solar sail system.

From the results, it is evident that the fundamental frequency of the solar sail is 0.00016 Hz, and the supporting CFRP boom remain undeformed, while the membrane exhibits significant deformation. This indicates the occurrence of local modes in the solar sail system, highlighting a severe stiffness mismatch among the system's components. In this case, the membrane has almost no out-of-plane stiffness, leading to considerable bending deformation.

For membrane structures, introducing in-plane prestress and forming a complete tension structure with the CFRP boom can significantly enhance their bending stiffness. For the structure designed in this study, the CFRP boom provide support at the vertices of the membrane. Therefore, adding prestress at the four corners of the square membrane is a reasonable approach, forming a corner-supported tension system.

Using the APDL module in ANSYS, the first-order frequencies of the solar sail structure under different prestress levels were calculated, and a mathematical surrogate model of the relationship between prestress and fundamental frequency was constructed. The results are shown in Fig. 7.

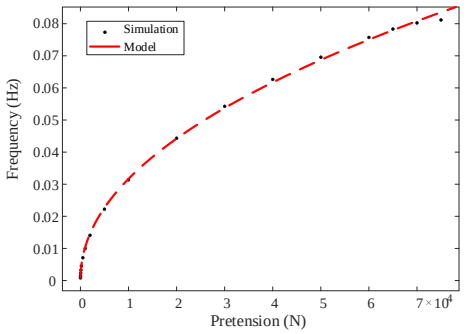

Fig. 7. Pretension plotted against frequency.

We adopted a power function fitting method to simulate the numerical trend. It is observed that before the prestress exceeds 70,000 N, the curve fitting performs exceptionally well, with an R-square value of 0.9998 and an RMSE value of 0.00046. Although this model does not fully describe the relationship between prestress and fundamental frequency, it is reasonably reliable within the threshold of 70,000 N. The expression for the surrogate model constructed using the power function is as follows:

$$f = 0.0003517 \cdot F^{0.4882} \quad (F \le 70000) \qquad (6)$$

where, f represents the natural frequency of solar sail and F represents the pretension added in the corner.

Moreover, from Fig. 7, the relationship between the fundamental frequency and prestress is clearly evident. As the pretension increases, the increment gradient of the fundamental frequency gradually decreases and eventually converges. However, when the pretension exceeds the threshold, the entire system becomes highly unstable because the CFRP boom, after bearing excessive force, undergo structural buckling.

After adding pretension, not only is the system's stiffness enhanced, but the stiffness of the internal components is more appropriately matched, resulting in a more rational configuration. At this point, the system no longer exhibits local modes. Taking a prestress of 1000 N as an example, the first four vibration modes and their frequencies are shown in Table 3 and Fig. 8.

Table 3. List of modal analysis results.

Mode	Frequency (Hz)	Deformation mode
1	0.0100	Bending (Symmetrical)
2	0.0140	Bending
3	0.0143	Bending
4	0.0172	Local deformation

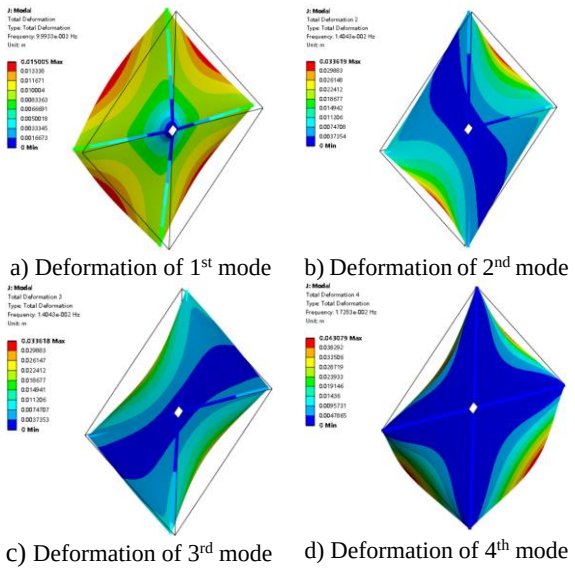

a) Deformation of 1st mode b) Deformation of 2nd mode

c) Deformation of 3rd mode d) Deformation of 4th mode

Fig. 8. Deformation mode of solar sail system

From Fig. 8, it can be observed that the first three modes of the system exhibit bending deformations. In the first mode, the deformation is a uniform bending of the entire structure in the negative direction along the membrane normal. In the second mode, one side of the structure deforms in the negative direction of the membrane normal, while the other side deforms in the positive direction. The third mode exhibits a deformation pattern that is symmetric to the second mode.

4. Conclusions

This paper presents a large deployable solar sail structure based on Flasher origami patterns. Utilizing a square Flasher origami pattern, the solar sail can be deployed in a clockwise direction. The folding mode of single-layer and double-layer pattern were analyzed, and the relationship between the folding mode and the number of layers of multi-layer square patterns was derived. Moreover, deployable CFRP boom extend concurrently with the sail surface during deployment, providing structural support and applying in-plane tension to enhance both in-plane and out-of-plane stiffness. The deploying process of the solar sail and CFRP boom was also displayed. Furthermore, modal analysis was conducted to examine the effect of prestress on the solar sail structure and to construct a mathematical surrogate model for the relationship between prestress and the fundamental frequency of the solar sail structure. Finally, the first four vibration modes and their corresponding deformations of the solar sail structure under the influence of prestress were analyzed.

References

[1]. Ghobakhloo, Morteza, and Masood Fathi. Industry 4.0 and opportunities for energy sustainability, *Journal of Cleaner Production*, 295, 2021, pp. 126427.

[2]. Baiocco, Paolo, Overview of reusable space systems with a look to technology aspects, *Acta Astronautica*, 189, 2021, pp. 10-25.

[3]. Duan, Fuqiang, Hongyi Xie, and Franco Bernelli-Zazzera, RCDs-based Feedback Control of a Solar Sail Spacecraft at the Earth-Sun L1 Point with Dual Pointing Requirements, in *Proceedings of the International Astronautical Congress: IAC Proceedings*, Milan, Italy, 2024, pp. 1792-1801.

[4]. Periola, Ayodele, Akintunde Alonge, and Kingsley Ogudo. Space habitat data centers—for future computing, *Symmetry*, 12, No. 9, 2020, p. 1487.

[5]. Y. Wu, et al., Reinforcement learning in dual-arm trajectory planning for a free-floating space robot, *Aerospace Science and Technology*, 98, 2020, p. 105657.

[6]. M. Zheng, et al., Reinforcement learning strategy for spacecraft attitude hyperagile tracking control with uncertainties, *Aerospace Science and Technology*, 119, 2021, p. 107126.

[7]. Y. Mao, et al., Dynamic Management Topology Construction, Evolution and Maintenance of LEO Mega-Constellation, *Space: Science and Technology*, 2025.

[8]. Y. Jiang, et al., Mega-constellation situational awareness mission planning with multi-constraints. *Systems Engineering and Electronic*, 2025.

[9]. Gonzalo, Juan Luis, Camilla Colombo, and Pierluigi Di Lizia. Analytical framework for space debris collision avoidance maneuver design, *Journal of Guidance, Control, and Dynamics*, 44, No. 3, 2021, pp. 469-487.

[10]. Frontier supercomputer, https://www.ornl.gov/news/frontier-supercomputer-debuts-worlds-fastestbreaking-exascale-barrier.

[11]. Hasan, Muhammad Noman, Muhammad Haris, and Shiyin Qin, Fault-tolerant spacecraft attitude control: A critical assessment, *Progress in Aerospace Sciences*, 130, 2022, pp. 100806.

[12]. Chen, Penghao, Xiaoli Luan, and Fei Liu. MT-filters- based event- triggered adaptive prescribed performance tracking control of multi- agent systems with unknown direction actuator failure, *International Journal of Robust and Nonlinear Control*, 33, No. 14, 2023, pp. 8224-8253.

[13]. Duan, Fuqiang, Hongyi Xie, and Franco Bernelli Zazzera, Fault-tolerant Orbit and attitude control of Solar sail with a rapid inspection and repair strategy of faulty RCDs, in *Proceedings of the Aerospace Europe Conference 2023, Joint 10th EUCASS - 9th CEAS Conference*, Lausanne, Switzerland, 2023, pp. 1-12.

[14]. Duan, F., Hongyi Xie, and Franco Bernelli Zazzera. Observer-Based Fault-Tolerant Integrated Orbit-Attitude Control of Solarsail, in *Proceedings of the Proceedings of the International Astronautical Congress: IAC Proceedings, Baku, Azerbaijan*, 2023, pp. 2-6.

[15]. Chen Y, Gu Y Q., Review on origami kinematics, *Advances in Mechanics*, 53, 1, 2023, pp. 154-197.

[16]. Lang, Robert J., Spencer Magleby, and Larry Howell, Single degree-of-freedom rigidly foldable cut origami flashers, *Journal of Mechanisms and Robotics*, 8, 3, 2016, p. 031005.

[17]. Mori, Osamu, et al., Improvement of sail storage and deployment mechanism for spin-type solar power sail, *Astrodynamics*, 4, 2020, pp. 223-231.

[18]. Scheel, H., Space-Saving Storage of Flexible Sheets, *U.S. Patent No. 3,848,821*, 1974.

[19]. Cai, Jianguo, et al., Mobility and kinematic paths of foldable origami structures, in *Proceedings of the International Design Engineering Technical Conferences and Computers and Information in Engineering Conference*, American Society of Mechanical Engineers, Vol. 50169, 2016, V05BT07A046.